The effect of alkylation on the micro-solvation of ethers revealed by highly localized water librational motion

Mihrin, D.; Voute, A.; Jakobsen, P. W.; Feilberg, K. L.; Larsen, R. W.

Published in:
The Journal of Chemical Physics

Link to article, DOI:
10.1063/5.0081161

Publication date:
2022

Document Version
Peer reviewed version

The Effect of Alkylation on the Micro-Solvation of Ethers Revealed by Highly Localized Water Librational Motion

D. Mihrin,[1,2] A. Voute,[2] P. W. Jakobsen,[2] K. L. Feilberg,[1] and R. Wugt Larsen[2]
[1)] *Danish Hydrocarbon Research and Technology Centre, Technical University of Denmark, Elektrovej 375, 2800 Kgs. Lyngby, Denmark*
[2)] *Department of Chemistry, Technical University of Denmark, Kemitorvet 206, 2800 Kgs. Lyngby, Denmark*

(*Electronic mail: rewl@kemi.dtu.dk)

(Dated: 14 January 2022)

The specific far-infrared spectral signatures associated with highly localized large-amplitude out-of-plane librational motion of water molecules have recently been demonstrated to provide sensitive spectroscopic probes for the micro-solvation of organic molecules [Mihrin *et al. Phys. Chem. Chem. Phys.* **21**, 1717 (2019)]. The present work employs this *direct* far-infrared spectroscopic approach to investigate the non-covalent intermolecular forces involved in the micro-solvation of a selection of seven ether molecules with systematically varied alkyl substituents: dimethyl ether, diethyl ether, diisopropyl ether, ethyl methyl ether, *t*-butyl methyl ether and *t*-butyl ethyl ether. The ranking of the observed out-of-plane water librational band signatures for this selected series of ether–water complexes embedded in inert neon matrices at 4 K reveals information about the interplay of directional intermolecular hydrogen bond motifs and non-directional and long-range dispersion interactions for the micro-solvated structures. These far-infrared observables differentiate minor subtle effects introduced by specific alkyl substituents and serve as rigorous experimental benchmarks for modern quantum chemical methodologies of various levels of scalability, which often fail to accurately predict the structural variations and corresponding vibrational signatures of the closely related systems. The accurate interaction energies of the series of ether–water complexes have been predicted by the local coupled-cluster approach DLPNO-CCSD(T) followed by a local energy decomposition analysis of the energy components. In some cases the secondary dispersion forces is in direct competition with the primary intermolecular hydrogen bonds as witnessed by the specific out-of-plane librational signatures.

I. INTRODUCTION

The large-amplitude out-of-plane hindered rotational motion of individual water molecules introduced upon complexation has proven enormously important for the unique hydrogen bond network rearrangement dynamics in liquid water[1,2] and even in the smallest of the water clusters[3–7]. The associated vibrational fundamental transitions occurring in the experimentally challenging far-infrared spectral region is the most prominent spectroscopic manifestation of hydrogen-bonded water molecules. The distinct far-infrared spectroscopic observables associated with this highly localized out-of-plane librational motion of individual water molecules have recently been shown to provide very sensitive spectroscopic probes for the hydrogen bond acceptor capabilities of importance for micro-solvation processes of alcohol molecules[8,9] and several other classes of organic molecules[8]. The intermolecular out-of-plane librational motion of the first solvating water molecule causes a significant change of dipole moment and gives rise to a strong characteristic far-infrared band correlated quantitatively with the complexation energy. The conventional relationship between the complexation energies and spectral red-shifts of the intramolecular OH stretching bands relative to the free water molecule observed in the mid-infrared region is less well defined for hydrated systems owing to the more effective decoupling of the two OH stretching modes of water as the intermolecular hydrogen bonds become stronger.

In the present work, this far-infrared cluster spectroscopy approach supported by theoretical interaction energy decomposition methodologies has been employed to explore the effect of specific alkyl substituent composition on the intermolecular forces involved in the micro-solvation processes for a variety of aliphatic ethers. The $+I$ inductive effect is one of the fundamental forces in which molecular surroundings influence the hydrogen bond donor-acceptor capability of a molecule, which in turn govern macroscopic phenomena as solvation processes[10]. In the case of non-linear molecular complexes, the dispersion interactions with bulky alkyl substituents are furthermore expected to compete with the intermolecular hydrogen bonds and affect the overall stabilities of the molecular complexes[11,12]. Quantum chemical methodologies in general struggle to provide quantitative descriptions of this interplay between different classes of non-covalent interactions, which are all critically important in both the energy, materials and life sciences. Rigorous experimental benchmarking of such intermolecular energy balances are thus crucial both for the validation and future development of modern theoretical methods.

Aliphatic ethers are excellent model systems for the classical intermolecular O-H···O hydrogen bonding type. These compounds have the R-O-R' motifs, resulting in higher sensitivity to the inductive effect compared to e.g. ketones. The selected sample set expands upon previ-

ously acquired experimental data sets on various alcohol-water complexes and is still within reach for accurate quantum chemical approaches. As the structurally related ether–water complexes have two alkyl groups substituted to the O atoms of the hydrogen bond acceptor motifs instead of one, the joint investigation of symmetric and asymmetric ether molecules with the same number of electrons, e.g. diethyl ether and methyl propyl ether, may shed further light on the competition between the different intermolecular forces. The experimental data sets on ether–water mixtures are of value themselves, as many of the ethers addressed in the present investigation are widely used in industry[13] and are useful in many applications such as organic synthesis[14], extraction of natural compounds, oil production[15], etc.

II. METHODOLOGIES

A. Experimental Details

The diethyl (DEE), diisopropyl (DIPE), *tert*-butyl methyl (TBME), *tert*-butyl ethyl (TBEE), and propyl methyl (PME) ethers of HPLC grade (¿99.9%, inhibitor-free) were purchased from Sigma-Aldrich. Several millilitres of the liquid were sampled into a glass vial fitted with a PTFE stopcock containing activated molecular sieves 4A. The samples were all degassed under vacuum at about -50°C to remove the dissolved air and minor traces of CO_2.

The dimethyl ether (DME) gas (99.9%, Sigma Aldrich) was transferred from a lecture bottle into a glass volume and further distilled from traces of air by a series of LN_2 freeze-pump-thaw cycles. For sample preparation, DME was nitrogen-cooled and transferred at the sublimation pressure. Ethyl methyl ether (EME) was prepared in house according to the Williamson method[16,17] from ethyl bromide and a sodium methoxide solution in methanol, with the product vacuum distilled in a LN_2 trap. The water samples were prepared by placing a few millilitres of Milli-Q grade water in a glass vial fitted with a vacuum valve and degassing under vacuum.

The setup for far-infrared matrix isolation spectroscopy consists of an immersion helium cryostat in conjunction with a Bruker IFS 120 HR FTIR spectrometer. The cryostat contains a rotatable vacuum shroud with positions for a CsI window and a gate valve for the inlet system. The inert gas matrix was obtained by simultaneous deposition of neon gas (99.999%, Air Liquide) with the sample vapour through separate inlet tubes onto a gold plated oxygen-free high thermal conductivity copper mirror at 3 K. The experimental sensitivity was increased by means of a specially designed dual-pass optical arrangement guiding the focused probe beam onto and back from the cold copper mirror of the cryostat and has previously been employed for investigations of weakly bound molecular complexes[18–20]. The neon was supplied via a MKS mass flow controller at 8 sccm flow rate, passing a LN_2-cooled spiral, depositing approximately 20 mmol of host gas per hour. The sample gas was supplied through a small-flow needle valve from a 5 litre glass volume. For all the matrix isolation experiments, the volume was filled with approximately 2 mbar of the respective ether sample and approximately 0.5 mbar of water vapor unless stated otherwise. The setup provided spectra in the mid-infrared range (650-4000 cm^{-1}, spectral resolution of 1.0 cm^{-1}) employing the combination of a water-cooled globar light source, Ge on KBr beam splitter and a semiconductor HgCdTe detector, as well as the far-infrared range (150-650 cm^{-1}) employing the source together with a 6 μm multilayer Mylar beam splitter and a liquid helium cooled Si-bolometer.

A complementary setup was used to acquire mid-infrared spectra down to 400 cm^{-1} for some of the systems without the consumption of liquid helium. This setup is based around a closed-cycle Advanced Research Systems (ARS) Cryo DE-204 4 K cryostat with a CsI cold window for measurements in transmission mode. The inlet system designed for this cryostat is analogous to the system described above. The mid-infrared spectra of doped neon matrices obtained with this setup were recorded by a Bruker Vertex 80V spectrometer, equipped with a broadband MCT detector, Ge on KBr beam splitter and an air-cooled globar source.

Following the acquisition of the initial spectra of the neon matrices (denoted pre-annealing spectra), the matrices were annealed by raising the temperature to 8.5 K for 10 minutes using a resistive heater and a Si-diode temperature sensor attached to the sample holder. As the cryogenic neon host medium is heated gently, the light water molecules diffuse in this softer environment and enable the micro-solvation of ether molecules in neighboring matrix cages. At the end of annealing, the matrices were all allowed to cool before the post-annealing sample spectra were recorded. The background spectra were collected for the evacuated cryostats with the clean sample mirror/window in the same optical arrangements at room temperature.

B. Computational Details

The quantum chemical calculations were performed using the ORCA (v.4.1)[21]. Potential energy minima structures and corresponding harmonic vibrational frequencies of the ether-water molecular complexes and their constituting fragments were calculated using the MP2[22] method with an aug-cc-pVQZ[23] (AVQZ) basis set. The resolution of the identity approximation was used for the MP2 and SCF integrals together with the numerical "chain-of-spheres X"[24,25] approximation and appropriate fitting basis sets[26–29] for both the energy and gradients. Partial atomic charges were calculated with the CHELPG method[30] using COSMO[31] radii.

The electronic dissociation energies (D_e) of the complexes were obtained by performing the domain based lo-

cal pair natural orbital coupled cluster method (DLPNO-CCSD(T))[32,33] single point calculations, with the aug-cc-pV5Z basis set and the RI-JK approximation, on the respective MP2 geometries. The cut-offs were set using the TightPNO keyword[34]. The zero-point energy corrected dissociation energies (D_0) of the binary complexes were calculated as the sum of the DLPNO-CCSD(T) electronic dissociation energies and the respective harmonic ΔZPE values from the MP2 calculations. The interaction energies of the complexes were analysed with the DLPNO-based local energy decomposition (LED) scheme. This procedure is described in details in the literature[35,36].

III. EXPERIMENTAL RESULTS

The following sub-sections contain detailed analyses of the experimental far-infrared spectra collected for the selection of ether-water systems. The complete list of band assignments for the investigated systems are given in Table I together with corresponding calculated structural parameters and harmonic vibrational frequencies.

A. Diethyl Ether (DEE) - Water

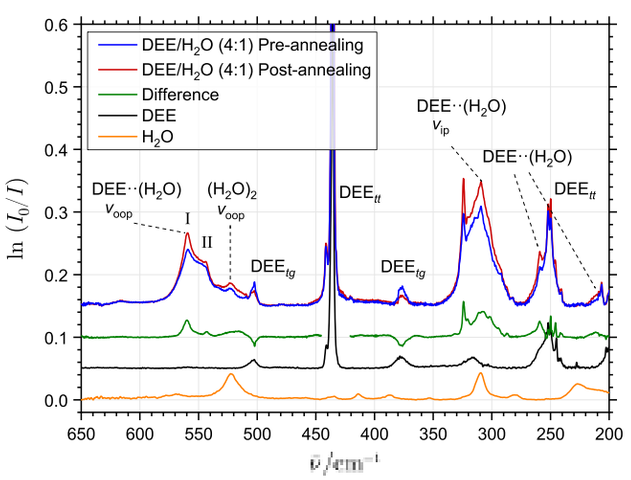

FIG. 1. The far-infrared absorption spectra collected before (blue trace) and after annealing to 9 K (red trace) for a mixture of DEE and water (mixing ratio of 4:1:600) and reference spectra of DEE (black trace) and water (orange trace) all embedded in solid neon. The green trace indicates the difference between the pre- and post-annealing spectra and the proposed assignments of the out-of-plane ν_{oop} and in-plane ν_{ip} librational bands for both the DEE·H_2O complex (the two different conformations are labelled I, II) and the water dimer are indicated together with band assignments for the DEE monomer conformations denoted DEE_{tg} and DEE_{tt}.

Fig. 1 shows the far-infrared absorption spectra (200–650 cm^{-1}) collected for cryogenic neon matrices doped with pure water (H_2O:Ne) = (1:600), pure diethyl ether (DEE:Ne) = (1:600) and mixtures of water and diethyl ether (H_2O:DEE:Ne) = (1:4:600) at 4 K. The far-infrared spectrum collected for DEE embedded in neon alone reveals a series of distinct bands at 202, 245, 252, 315, 378, 436, 441 and 502 cm^{-1}. These bands have all previously been assigned to fundamental transitions associated with intramolecular skeleton bending motion (202 cm^{-1}), large-amplitude C-CH_3 torsional motion (245 and 252 cm^{-1}), skeleton deformation motion (378 and 502 cm^{-1}), anti-phase CCO bending motion (436 cm^{-1}) and COC bending motion (441 cm^{-1}) for two energetically close *trans-trans* (denoted DEE_{tt}) and *trans-gauche* (denoted denoted DEE_{tg}) conformations of DEE. The detailed vibrational assignments including the torsional-vibrational anharmonic coupling of modes for these DEE conformations are beyond the scope of the present contribution and we refer to the scientific literature for additional information[37,38]. The far-infrared spectrum of pure water embedded in neon alone reveals several bands previously assigned to water dimer and water trimer. The chosen H_2O:Ne mixing ratio favours mostly dimer formation and, to a lesser extent, trimer formation. The band observed at 309 cm^{-1} is associated with the donor in-phase librational mode (*c*-type librational motion) of water dimer, whereas the band at 522 cm^{-1} is associated with the highly localized out-of-plane librational mode of water dimer[39]. The series bands observed from 450 to 350 cm^{-1} and the band at 280 cm^{-1} in the reference spectrum of pure water in neon have all previously been assigned to vibrational fundamentals associated to librational motion of the cyclic water trimer[40,41]. These bands vanish completely in the spectrum collected when both DEE and water are co-deposited in neon due to the effective quenching of water trimer formation with 4:1 excess of DEE in the matrix relative to water.

For the neon matrices doped simultaneously with water and DEE, several new bands appear in the far-infrared spectrum in close vicinity to the donor OH librational bands of water dimer. Two overlapped but still distinct bands are observed at 559.7 cm^{-1} and 542.7 cm^{-1} and thereby with significantly higher band origins than the large-amplitude intermolecular out-of-plane librational band of water dimer (522 cm^{-1}). At the same time, a new broad band with less apparent sub-band structure is observed around 310 cm^{-1} and thereby strongly overlapped both with the transitions assigned to the large-amplitude intermolecular in-phase *c*-type libration of water dimer (309 cm^{-1}) and the intramolecular CCO bending mode of DEE at 315 cm^{-1}. In addition, a fourth new band is observed at 259 cm^{-1} and slightly blue-shifted relative to the free C-CH_3 torsional band of DEE_{tt} assigned at 252 cm^{-1}. The new bands all gain significant intensity upon annealing up to 9 K and are for that reason assigned to mixed molecular complexes of DEE and water. The annealing procedure promotes the diffusion of the light water molecules in the soft neon environment above 7 K, favouring the formation of complexes[39]. The two dis-

tinct bands at 559.7 cm^{-1} and 542.7 cm^{-1} are straightforwardly assigned to transitions associated with the highly localized out-of-plane librational modes of the 1:1 complex of DEE and water. The improved hydrogen bond acceptor capability of DEE strengthens the intermolecular hydrogen bond between DEE and water relative to the hydrogen bond in water dimer. The out-of-plane librational band origins are expected to follow the trend reported in our previous far-infrared investigations concerned with hydrogen-bonded alcohol-water complexes[8]. The observation of two distinct out-of-plane librational bands clearly points at two different conformations of the DEE·H_2O complex with slightly different hydrogen bond orientations. This is also supported by the annealing procedure indicating that the less stable conformation of the complex with band origin at 542.7 cm^{-1} is formed slower than the more stable conformation with band origin at 559.7 cm^{-1}, compared to the pre-annealing ratio between the two forms. The new broad band around 310 cm^{-1} and the band at 324 cm^{-1} must then be assigned to the in-phase *c*-type librational transitions expected for the two conformations of the DEE·H_2O complex. The final new band observed at 259 cm^{-1} may then be assigned to transitions associated with the slightly perturbed C-CH_3 torsional modes of the DEE·H_2O complex picking up infrared intensity from the dipole moment change of the hydrogen-bonded water molecule.

The annealing procedure further distinguishes features associated with the *trans-gauche* isomer of DEE. The positions of the bands (502 and 376 cm^{-1}) are in agreement with the literature, but the relative abundance of the conformers is significantly shifted compared to estimates at ambient temperature[38,42], and annealing of the matrix further induces relaxation of the remaining *trans-gauche* DEE molecules into the *trans-trans* conformation. This experimental evidence indicates that the two observed conformations of the DEE complex with water differ in the way of how water molecule is attached to DEE in the *trans-trans* conformation, rather than due to different conformations of the DEE fragment itself. The potential energy minima structures of the different conformations will be investigated computationally in section IV A.

B. Diisopropyl Ether (DIPE) - Water

Fig. 2 shows the far-infrared absorption spectra (200-650 cm^{-1}) collected for cryogenic neon matrices at 4 K doped with pure water (H_2O:Ne) = (1:600), pure diisopropyl ether (DIPE:Ne) =(1:600) and a mixture of water and diisopropyl ether with a mixing ratio of (H_2O:DIPE:Ne) = (1:4:600).

The band associated with the low-frequency COC bending mode is observed at 202 cm^{-1} and the two bands associated with the in-phase and out-of-phase CCC bending modes are located at 301 cm^{-1} and 390 cm^{-1} for the DIPE monomer, respectively. The bands at 407 cm^{-1} and 428 cm^{-1} correspondingly are assigned to the COC

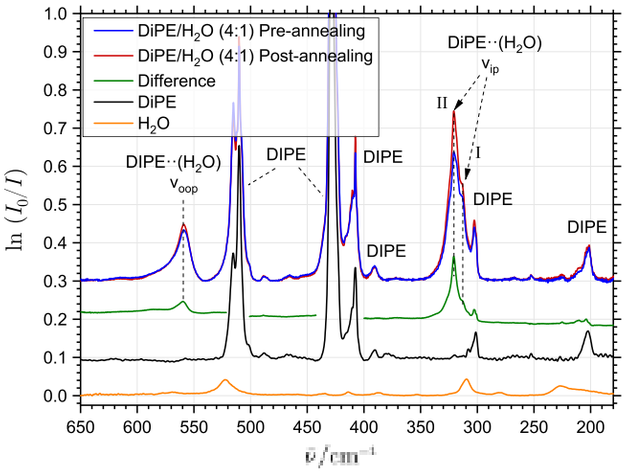

FIG. 2. The far-infrared absorption spectrum collected before (blue trace) and after annealing (red trace) of a mixture of DIPE and water embedded in neon with mixing ratio of 4:1:600 and the corresponding reference spectra of pure DIPE (black trace) and pure water (orange trace). The green trace indicates the difference between the pre- and post-annealing spectra and the proposed assignments of the out-of-plane (ν_{oop}) and the in-plane (ν_{ip}) librational bands for the DIPE·H_2O complex (the two different conformations are labelled I, II) are indicated together with band assignments for the DIPE monomer.

twisting and wagging modes of DIPE, the weak 488 cm^{-1} band is assigned to the COC bending mode and the band at 510 cm^{-1} is assigned to the CCCO umbrella mode of DIPE. The band at 515 cm^{-1} should likely be assigned to the umbrella mode of a less stable DIPE conformation. These observations in the solid neon environment are in qualitative accordance with previous investigations of both thin films[43], the liquid phase[44] and the gas phase[45].

The relevant ν_{oop} band for the respective DIPE·H_2O complex is clearly observed at 559.6 cm^{-1}, nearly at the same position as has been found for the similar DEE·H_2O complex, however, only one single slightly asymmetric broad band is observed for the DIPE·H_2O system. At 320.7 cm^{-1} an intense band with a shoulder around 313 cm^{-1} is observed. These bands are assigned to the in-plane librational mode ν_{ip} of two different conformations of the DIPE·H_2O complex. Evidently, the structural differences between the two conformations have a stronger influence on this *c*-type water librational mode (the hindered overall rotation of the water molecule) than the highly localized ν_{oop} mode where only the donor H atom is engaged. Upon annealing, the spectral subtraction between the post- and pre-annealing spectra shows a substantial growth of intensity of the 320.7 cm^{-1} absorption supporting that this transition should be assigned to the in-plane librational mode of the most stable DIPE·H_2O conformation.

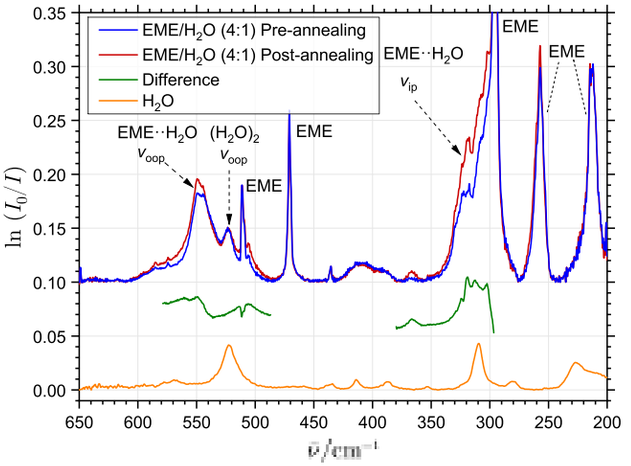

FIG. 3. The far-infrared absorption spectra collected before (blue trace) and after annealing (red trace) of a mixture of EME and water embedded in solid neon with mixing ratio of 3:1:600 together with a reference spectrum of water (orange trace). The green trace indicates the difference between the pre- and post-annealing spectra and the proposed assignments of the out-of-plane (ν_{oop}) and the in-plane (ν_{ip}) librational bands for the EME·H_2O molecular complex are indicated together with band assignments for the EME monomer conformations.

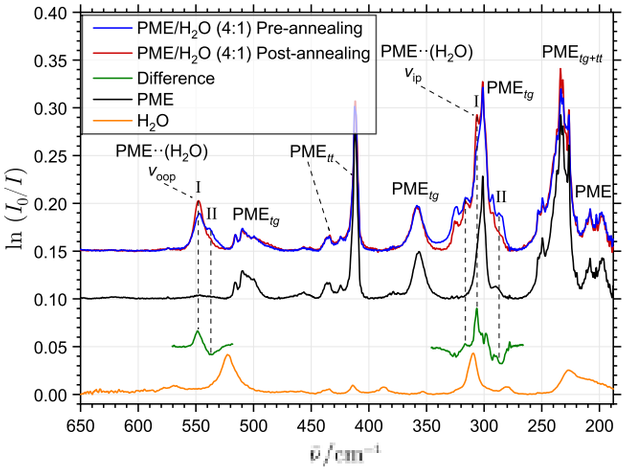

FIG. 4. The infrared absorption spectra collected before (blue trace) and after annealing (red trace) of a mixture of PME and water embedded in solid neon with mixing ratio of 4:1:600 together with a reference spectrum of PME (black trace) and water (orange trace). The green trace indicates the difference between the pre- and post-annealing spectra and the proposed assignments of the out-of-plane ν_{oop} and in-plane ν_{ip} librational bands for the PME·H_2O complex (the two different conformations are labelled I, II) are indicated together with band assignments for the PME monomer conformations.

C. Ethyl Methyl Ether (EME) - Water

Fig. 3 shows the far-infrared spectra for the neon matrices doped with pure water (H_2O:Ne = 1:600) and a mixture of ethyl methyl ether with water having a mixing ratio of (EME:H_2O:Ne = 3:1:600). The bands observed in the spectra at 213 and 256 cm^{-1} should be assigned to the two O-CH_3 torsional modes, the bands at 296 and 471 cm^{-1} should be assigned to the in-phase and out-of-phase hybrid CCO and COC bending modes of EME, respectively[46,47]. The band at 511 cm^{-1} has not previously been observed in the gas phase. Kitagawa *et al.*[46] have estimated the *gauche* conformation of EME to have the bending band at 510 cm^{-1}. This band exhibits a reversed annealing effect (less band intensity in the post-annealing spectrum) in agreement with other monomer bands in the spectrum, suggesting that it might potentially be due to a combination of the 213 and 296 cm^{-1} bands.

The remaining observed bands are assigned to water clusters and the mixed EME·H_2O complex. The broader structured band with an origin at ~313 cm^{-1} is assigned to the in-plane librational mode ν_{ip} and finally the band with maximum at 549.1 cm^{-1} is assigned to the target out-of-plane librational mode ν_{oop} of the complex. As expected from the previously established trend among homologous ether-water complexes, the band position is lower than found for the DEE·H_2O complex, indicating a lower hydrogen bond acceptor capability of the EME molecule relative to DEE. In contrast to the DEE·H_2O system, only a single conformation of this complex was detected for this system.

D. Propyl Methyl Ether (PME) - Water

Fig. 4 shows the infrared spectra for neon matrices doped with pure water (H_2O:Ne = 1:600), a mixture of propyl methyl ether with water having a mixing ratio of (PME:H_2O:Ne = 4:1:600) and a spectrum of pure PME (PME:Ne = 1:200). The observed bands with maxima at 509 and 516 cm^{-1} are associated with the COC bending/CH_2 rocking motion of the *trans-gauche* conformation. The bands at 434 and 412 cm^{-1} band are assigned to the COC and CCC bending modes of the *trans-trans* conformation[48]. The bands at 356 cm^{-1} and 301 cm^{-1} are associated with twisting modes of the *trans-gauche* conformermation. The band at 233 cm^{-1} is associated with CH_3-O torsions of both conformers and the weak absorption features at 208 cm^{-1} and 197 cm^{-1} are associated with CH_3-C torsional (*trans-gauche*) and skeletal deformation motions (*trans-trans*), respectively.

The out-of-plane librational band ν_{oop} of the most stable conformation of the PME·H_2O complex is assigned at 547.3 cm^{-1}. This very distinct band has a reproducible shoulder around 537.2 cm^{-1} in the pre-annealing spectrum, which is significantly reduced in intensity in the post-annealing spectrum. The difference spectrum clearly reveals the relaxation of the less stable conformation (intensity decrease of the 537.2 cm^{-1} band) into the

global potential energy minimum (intensity increase of the 547.3 cm^{-1} band). This trend is supported by the observations in the region of the in-plane librational motion ν_{ip}. A distinct band at 306 cm^{-1} shows strong positive annealing effect, matching this band with the 547.3 cm^{-1} band of the global minimum conformation, whereas a band around 287 cm^{-1} decreases in intensity upon annealing indicative of the local potential energy minima. As all the detected out-of-plane librational bands ν_{oop} are located above 500 cm^{-1}, the remaining of the selected ether-water systems are solely presented in the spectral region down to 400 cm^{-1}.

E. tert-Butyl Methyl Ether (TBME) - Water

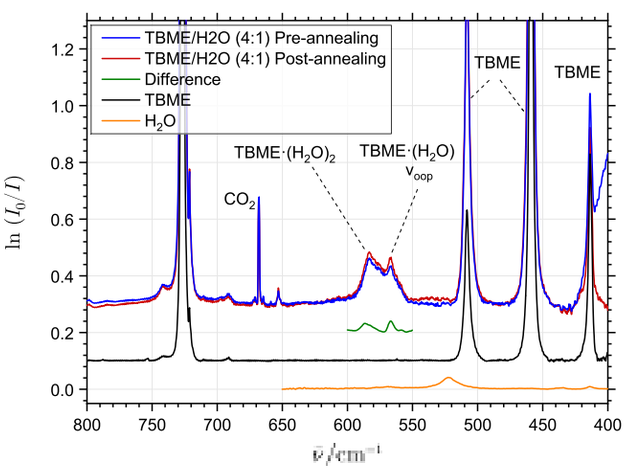

FIG. 5. The infrared absorption spectra collected before (blue trace) and after annealing (red trace) of a mixture of TBME and water embedded in solid neon with mixing ratio of 4:1:600 together with a reference spectrum of TBME (black trace) and water (orange trace). The green trace indicates the difference between the pre- and post-annealing spectra. The proposed assignment of the out-of-plane (ν_{oop}) librational band for the TBME·H_2O complex is indicated together with band assignments for the TBME monomer. The band located near 580 cm^{-1} is tentatively assigned to the ternary TBME·$(H_2O)_2$ complex.

Fig. 5 shows the infrared spectra (400-800 cm^{-1}) for the neon matrices doped with a mixture of *tert*-butyl methyl ether with water (TBME:H_2O:Ne = 4:1:600), pure water (H_2O:Ne = 1:600) and pure TBME (H_2O:Ne = 1:150). There is scarcity of information about the vibrational spectrum of TBME below 700 cm^{-1}, however, our theoretical harmonic predictions as described in section IV A are in excellent agreement with our matrix experiment in the 300-700 cm^{-1} spectral range. The TBME monomer bands located at 414 cm^{-1}, 459 cm^{-1} and 508 cm^{-1} should be assigned to the *tert*-butyl substituent's umbrella mode, COCC skeletal deformation and the COC bending motion, respectively. The band at 726 cm^{-1} should be assigned to the *tert*-butyl breathing motion[49]. The far-infrared bands at 371 cm^{-1} and 346 cm^{-1} are assigned to the COC/CCC bending motion and the CCCC asymmetric bending motion of the *tert*-butyl group, respectively. The two broad bands related to mixed complexes are present in the range of the spectrum where the out-of-plane librational band ν_{oop} is expected for the respective binary system. These two bands have been reproduced in experiments with several mixing ratios (8:1:1200 to 1:1:300) but the bands exhibit different relative annealing responses. These intensity changes with annealing can be correlated with the two respective bands in the OH-stretching range of the spectrum (not shown), located at 3485 cm^{-1} and 3505 cm^{-1} corresponding to the far-infrared bands at 557 cm^{-1} and 587 cm^{-1}, respectively. Based on the combined annealing observations in the far- and mid-infrared spectra, we tentatively attribute the 587 cm^{-1} band to a ternary TBME·$(H_2O)_2$ and the band at 557 cm^{-1} to the target out-of-plane librational mode ν_{oop} of the binary TBME·H_2O system.

F. tert-Butyl Ethyl Ether (TBEE) - Water

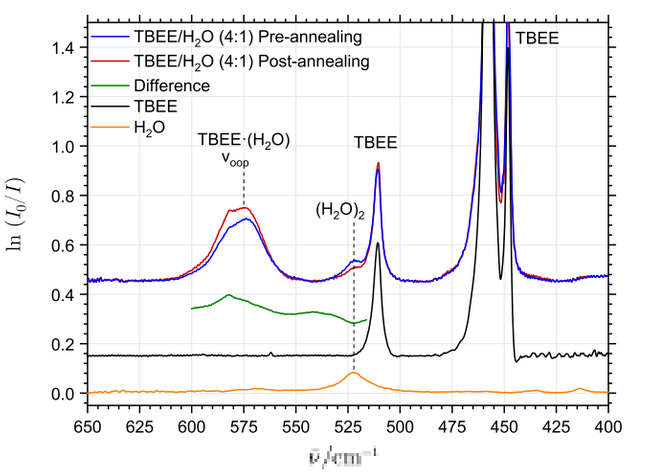

FIG. 6. The infrared absorption spectra collected before (blue trace) and after annealing (red trace) of a mixture of TBME and water embedded in solid neon with mixing ratio of 4:1:600 together with a reference spectrum of TBME (black trace) and water (orange trace). The green trace indicates the difference between the pre- and post-annealing spectra. The proposed assignment of the out-of-plane (ν_{oop}) librational band for the TBEE·H_2O complex is indicated together with band assignments for the TBEE monomer. The band located near 580 cm^{-1} is tentatively assigned to a ternary TBEE·$(H_2O)_2$ complex.

Fig. 6 shows the infrared spectra (400-800 cm^{-1}) for the neon matrices doped with a mixture of *tert*-butyl methyl ethe with water (TBEE:H_2O:Ne = 4:1:600), pure water (H_2O:Ne = 1:600) and pure TBEE (H_2O:Ne = 1:150). The 448 cm^{-1} and 457 cm^{-1} bands should be assigned to

out-of-plane deformation modes and the 511 cm^{-1} band is associated with to COC bending/*tert*-butyl umbrella motion of TBEE monomer[50]. Located near 580 cm^{-1}, only one structured band is observed in the range of the expected range for the out-of-plane librational mode of the TBEE·H_2O complex. The band is broad and asymmetric in the pre-annealing spectrum but the difference spectrum after annealing reveals growth of a more or less distinct band with maximum at 582.2 cm^{-1}. Additional experimental work would be required for an unambiguous confirmation of the proposed assignment but based on the similar findings for the TBME·H_2O complex, we believe that this band should likewise be attributed to a ternary TBEE·$(H_2O)_2$ system. The assumption that a water-rich ternary TBEE·$(H_2O)_2$ system is formed in the matrices upon annealing is somewhat reinforced by the observation that the number density of water dimers seems to go down simultaneously. The band origin for the out-of-plane librational band $\nu_{oop}$of the binary TBEE·H_2O complex is then estimated to be 574.5 cm^{-1}.

G. Dimethyl Ether (DME) - Water Revisited

In our recent work[8], the out-of-plane librational band of the DME·H_2O complex in the neon matrix environment was re-assigned at 555.9 cm^{-1}. This system is revisited again in light of the present extensive complementary experimental results for the series of homologous ether-water complexes. The DME·H_2O system was initially investigated by in several noble gas materials and the far-infrared assignments of the out-of-plane librational mode of this complex were proposed at 524.0, 555.9 and 547.4 cm^{-1} in doped neon, argon and krypton matrices, respectively.[51] The substantial shift from argon to neon matrices reported is not consistent with typically observed matrix spectral shifts associated and these observations do not follow the host material trend reported for the corresponding out-of-plane librational mode of the water dimer. In addition, this 524.0 cm^{-1} band assignment to the out-of-plane librational mode of the most stable conformation of the DME·H_2O complex seems too close to the assignment for water dimer at 522.4 cm^{-1} considering the substantial difference in interaction energies between the two complexes.[8]. Our recent experimental findings showed that, apart from the very broad 524 cm^{-1} band, a comparatively weak absorption could be found at 555.9 cm^{-1}. However, the present experimental assignments of the out-of-plane librational bands for the homologous ether-water complexes, namely EME·H_2O at 549.1 cm^{-1} and PME·H_2O at 547.3 cm^{-1} indicate that this very weak 555.9 cm^{-1} absorption also should not be assigned to the out-of-plane librational transition of DME·H_2O.

In our revisit of this system, we have performed a new series of experiments with a wide range of DME:H_2O:Ne mixing ratios ranging from 1:1:600 to 24:1:1200. The

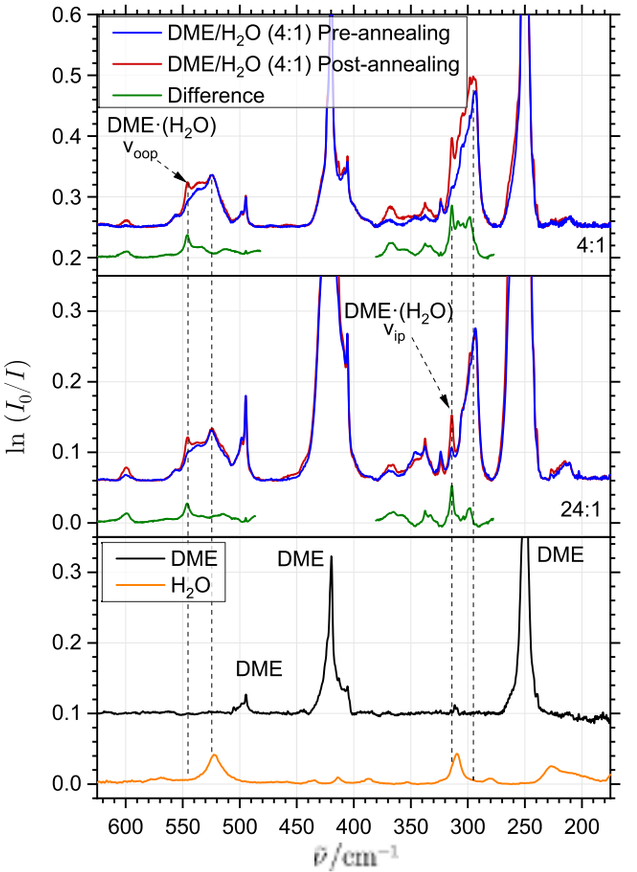

FIG. 7. The far-infrared absorption spectra of two different DME/water mixtures with mixing ratios of 4:1:600 (top) and 24:1:1200 (center) and corresponding reference spectra of pure DME (bottom, black trace) and pure water (bottom, orange trace) in solid neon. For each DME/water mixture, the pre-annealing spectra (blue traces) and post-annealing spectra (red traces) are shown together with the difference spectra in the relevant spectral regions (green traces). The proposed assignments for the out-of-plane (ν_{oop}) and the in-plane (ν_{ip}) librational bands of the global potential energy minimum of the DME·H_2O complex are indicated .

far-infrared spectra of these independent matrices are shown in Fig. 7 both before and after annealing together with the reference spectra of DME and water embedded in neon alone. The rather weak 555.9 cm^{-1} absorption is again reproduced in the spectra collected for both mixtures, as well as the broad band at 524 cm^{-1}. The annealing of both matrices, however, independently reveal the substantial growth of a third quite distinct band at 546.6 cm^{-1}, while the aforementioned absorption features show little to no growth. Remarkably, this new 546.6 cm^{-1} band is only seen as a weak shoulder in the pre-annealing spectra and only slightly more evident when DME is abundant in large excess. At the same time, we observe in the range of the in-plane librational mode, previously assigned for this complex at 293 cm^{-1},

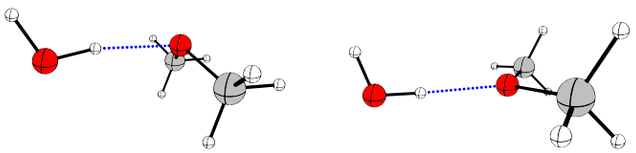

(a) Conformation A, global minimum

(b) Conformation B, local minimum

FIG. 8. The calculated structures of the two possible conformations of the DME·H_2O molecular complex

a strong and broad asymmetric band indeed appears at 293 cm^{-1}. On annealing of the matrix, this band however shows only minor growth. At the same time, a new distinct band emerges at 314 cm^{-1} as a shoulder in spectra with higher DME:H_2O mixing ratios and stands out clearly in the experiment with huge DME excess. This new band shows a pronounced annealing effect very similar to the behavior of the 546.6 cm^{-1} band. In addition, the 314 cm^{-1} band position agrees better with theoretical predictions for the in-plane librational transition of the global minimum for the DME·H_2O complex as will be evident in section IV A. Based on these new strong experimental annealing evidences, we then believe that all the reported observations can be explained by the presence of two different energetically close conformations of the DME·H_2O complex.

In the investigation on the similar DME·methanol complex by Han[52], the authors reported experimental evidences suggesting the presence of two different conformations. The difference between the two ways the hydrogen bond donor molecule can attach DME can be viewed as the relative orientation of the unbound side of the donor fragment. The two calculated potential energy minima structures in Fig. 8 represent our best attempts to capture these two conformations for the DME·H_2O complex. While both the conformational wells in the DME·methanol complex probably are well defined, owing to the additional dispersion interactions from the methyl group, the energy barrier between the two similar conformations of the DME·H_2O complex is expected to be smaller. The implication is that the local minimum cannot be reliably captured computationally at higher levels of theory. Nevertheless, at the DFT-level we have still predicted the difference in the out-of-plane librational band origin for the two conformations to be about 20 cm^{-1} in the harmonic approximation close to the experimental findings. Based on these considerations, we assign the newly observed bands at 546.6 and 314.0 cm^{-1} as the out-of-plane and in-plane librational modes, respectively, for the global minimum conformation (conformation A), while the previous assignments by Engdahl and Nelander could be attributed to the less stable conformation of the complex (conformation B).

IV. SUPPORTING THEORETICAL RESULTS AND DISCUSSIONS

A. Intermolecular Potential Energy Minima and Structural Parameters

To aid the interpretation of the present experimental data sets, the present results have been supported by *ab initio* calculations of the potential energy minima structures and the corresponding harmonic vibrational spectra for all systems at the MP2/AVQZ level of theory. For some of the systems, only one conformation was found at this computational level and all of these systems were found to be clearly hydrogen-bonded complexes with water serving as the hydrogen bond donor. The relevant structural parameters such as intermolecular hydrogen bond lengths and O-H···O angles were calculated, as well as the partial charges located on the O atoms of the hydrogen bond accepting ether molecules. The computational results are presented in Table I together with the corresponding values for the previously investigated hydrogen-bonded alcohol-water complexes.

Multiple potential energy minimum conformations were found for some of the ether-water systems. For the mono-hydrated complexes of the linear DEE, EME and DME molecules two conformers associated with a different rotation of the water molecule along the hydrogen bond were optimised (see Fig. 8). The conformations of type B are less stable and have lower calculated out-of-plane librational band positions than the respective type A conformations. For the DEE·H_2O system, the harmonically predicted out-of-plane librational band origin of the conformation B is 18 cm^{-1} lower than for the conformation A, explaining the two observed bands in the corresponding matrix experiment. This isomerism is less likely for the asymmetric linear ether molecules as the interaction with the larger substituent may facilitate rotation of the water fragment. For the PME·H_2O system, the found conformations are also associated with two rotamers of the alkyl chain, both of which to a varying degree can form complexes with water in type A and B conformations. The calculations suggest that two possible *trans-trans* and *trans-gauche* conformations of the PME·H_2O complex (Fig. 9) are extremely close in energy. The experimental findings suggest that we observe both conformations of the PME·H_2O complex as evidenced by the very clear annealing behaviour of both the observed out-of-plane and in-plane librational band contours. The annealing results seem to confirm that it is the *trans-gauche* form that is more stable in the PME·H_2O system under matrix conditions as evidenced by the order of the predicted harmonic librational band origins also for the in-plane librational band range. The distinct absorption band at 547.3 cm^{-1} is then assigned to the global *trans-gauche* minimum conformation and employed for the systematic trend analysis. Finally, two conformations of the DIPE·H_2O complex were found, differentiated by different mutual orientations of the substituents. The cal-

TABLE I. Summary of the computed relevant structural parameters at the MP2/AVQZ level of theory: the intermolecular hydrogen bond distances ($\boldsymbol{r}_{H\cdot O}$ in Å), the $\angle_{OH\cdot O}$ angles (in degrees), the CHELPG partial atomic charges (δ–O) on the O atom of the acceptor moiety, the harmonically predicted (ω_{oop}) and the experimentally assigned ($\nu_{\text{oop, exp}}$) out-of-plane librational band positions (in cm^{-1}) for the global potential energy minima of the investigated hydrogen bonded-complexes of water with aliphatic ethers, aliphatic alcohols together with the water dimer reference system.

Systems	Theoretical				
	δ–O	$\boldsymbol{r}_{H\cdot O}$	$\angle_{OH\cdot O}$	ω_{oop}	$\nu_{\text{oop, exp}}$
H_2O	0.73	1.943	171.7	628.0	522.4[39]
DME	0.19	1.867	164.8	653.2	546.6
EME	0.30	1.864	165.4	658.0	549.1
PME_{tg}	0.24	1.862	169.9	656.4	547.3
DEE	0.41	1.866	168.6	669.2	560.1
DIPE	0.59	1.858	168.8	667.8	559.6
TBME	0.45	1.848	167.4	685.4	567.0
TBEE	0.54	1.854	165.2	693.0	574.5
MeOH	0.62	1.893	164.7	634.4	527.5[53]
$EtOH_g$	0.68	1.888	161.6	642.6	551.6[9]
$EtOH_t$	0.68	1.896	165.6	651.5	545.4[9]
i-POH	0.73	1.896	164.8	656.5	554.3[8]
t-BuOH	0.77	1.885	165.7	662.7	556.4[54]

culated harmonic values for the out-of-plane librational transitions are almost identical for these conformations, however, there is slight spectral shift estimated for the in-plane librational transitions, confirming the experimental observations of two different forms in the 310-320 cm^{-1} spectral range.

These predicted structural parameters suggest that, in those cases where the bond angle deviates from the ideal linear 180° configuration, strong secondary interactions presumably of dispersive nature, is acting in competition with the primary hydrogen bond. The hydrogen bond angles of the DME·H_2O and EME·H_2O complexes are noticeably lower than calculated for the water dimer. The long-chained ethers such as PME pose an additional challenge for an accurate comparison to theory as the fully stretched conformation of the skeleton is not necessarily the most abundant as discussed above.[48]. Another observable effect is the twist of the water molecule in the PME·H_2O complex (Fig. 9). In contrast to the complex of a symmetric ether, e.g. the DME·H_2O system, the water molecule is turned with the oxygen closer to the larger substituent due to dispersive interaction of the water molecule with the alkyl substituent in competition with the hydrogen bond. The twist is also present in the calculated structure of the asymmetric EME·H_2O system but to a much smaller extent.

The inductive effect of the substituents falls off rapidly with bond count and the difference is almost negligible between the ethyl and propyl substituents. The partial

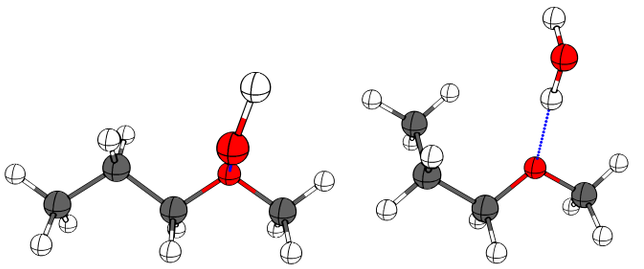

(a) *trans-trans* (b) *trans-gauche*

FIG. 9. The top-down view of the calculated potential energy minima structures of the PME·H_2O complex (MP2/AVQZ level of theory). The molecular plane of water is indicated in blue, demonstrating overall tilt of the molecule towards larger alkyl substituent of the PME subunit.

charge alone does not appear to provide sufficient information for the explanation of the experimental observations. It is clear that the high negative charge and the large bond angle found in water dimer are indicative of the dominant electrostatic component of this interaction. The theoretical vibrational frequencies generally correlate quite well with the experimental results with a scaling factor to the harmonic predictions of approximately 84%. However, the differences between closely positioned band origins of the DME·H_2O, EME·H_2O and PME·H_2O complexes are overestimated suggesting that an accurate treatment of electronic correlation plays an important role in a quantitative differentiation of the acceptor capability of this series of molecules.

B. Local Energy Decomposition of Complexation Energies

To investigate the interplay between the different classes of intermolecular forces more deeply, the interaction energies of the systems were analysed employing the local energy decomposition (LED) method, exploiting the local pair nature of the underlying DLPNO-CCSD model. The method has previously been tested on a set of diverse systems and has been applied for the analysis of the intermolecular forces of the water dimer[55].

The net dissociation energy of the complex (D_e) is decomposed into the geometry preparation energy ΔE_{geo}, the dispersive (pure dispersion $\Delta E^{SP}_{disp}, \Delta E^{WP}_{disp}$ is combined with the (T) component[36,56]) and the non-dispersive (electronic preparation $\Delta E^{HF}_{el.prep.}$, electrostatic and exchange $\Delta E^{HF}_{el-st+XC}$ terms, non-dispersive contributions from the CCSD pairs ΔE^{SP}_{res}) contributions. A detailed description can be found in the supplementary material and in the original publications[35,57]. The final fragmentation of the complete zero-point corrected dissociation energy (D_0) for a given ether-water complex we then select as:

$$D_0 = \Delta E_{geo} + \underbrace{\Delta E^{HF}_{el.prep.} + \Delta E^{HF}_{el-st+XC} + \Delta E^{SP}_{res}}_{\text{Non-dispersive}} + \underbrace{+ \Delta E^{SP}_{disp} + \Delta E^{WP}_{disp} + \Delta E^{(T)}}_{\text{Dispersive}} + \Delta ZPE \quad (1)$$

The results of the analysis are summarized in Table II. As can be expected, the water dimer complexation energy is heavily dominated by the non-dispersive component. The interaction energies of the mixed ether-complexes all show dramatically higher relative contributions from the dispersion component, increasing from approximately 30% for the water dimer to approximately 40% for the DME·H_2O complex and growing further as expected with the alkyl substituent sizes.

In the DME·H_2O–EME·H_2O–PME·H_2O sequence the total dissociation energy increases, converging with the alkyl substituent length. The non-dispersive component, however, can be seen to decrease, while the dispersion contribution increases. This suggests that the dispersion interaction is in competition with the electrostatic component. From the DME·H_2O to EME·H_2O systems, the drop of the non-dispersive energy is small compared to the increase of the dispersion, whereas going to the PME·H_2O system, the non-dispersive component decreases significantly. This is likely due to the fact that in the PME·H_2O complex, the dispersive forces act from a greater angle, straining the hydrogen bond. On the other hand, in the EME·H_2O complex and specifically in the DME·H_2O complex, the mean vector of dispersive force is more aligned with the hydrogen, so the reduction in the net non-dispersive component comes primarily from the increase in electrostatic repulsion. The latter is calculated to be identical for the EME·H_2O and PME·H_2O complexes but drastically lower for the DME·H_2O system. As the out-of-plane librational band position does not follow the dissociation energy for these complexes, the aforementioned effect can be seen as the one of the causes for this deviation.

In line with the conclusion, the symmetric DEE·H_2O complex shows an increase of both the net N/D interaction and the electrostatic preparation component over the PME·H_2O system. The librational band position for this complex is higher by 11 cm^{-1} than found for EME·H_2O, despite the fact that the dispersion ratio is increased to 50% over the 45% in the latter.

Both conformations of the DIPE·H_2O complex show an increase of the N/D and dispersive energy components, owing to the presence of two large branched substituents. However, the experimentally observed librational band position is nearly identical to that of the DEE·H_2O complex, also in agreement with the calculations. It is very likely that the specific surroundings of the water molecule is affecting the band position, as the ΔZPE for this complex is measurably higher than predicted for the DEE·H_2O

The TBME·H_2O complex shows the highest net non-dispersive interaction component of all the investigated ether-water complexes, almost on par with the value for the water dimer. However, a large portion comes from the CCSD charge-polarization component (SP_{res}). The dispersion component of the energy is somewhat below that of the DIPE system, as well as the total D_0. With the increase of the alkyl chain length in the TBEE·H_2O complex, most of the changes resemble the cases of the linear ethers. There is a reduction in the net N/D component, associated primarily with the rapid growth of the electrostatic repulsion outweighed by the increase in dispersive forces, while all other sub-components increase in magnitude as well. These differences manifest in a measurably higher librational band position for the TBEE·H_2O complex.

The set of previously studied alcohol-water complexes falls well into the newly acquired results, with a decent correlation between the theoretical dissociation energies of the complexes and their respective observed out-of-plane librational band positions. Each of the alcohol molecules forms a somewhat weaker complex with water than their respective ether analogue, e.g. t-BuOH·H_2O versus TBME·H_2O and $EtOH_t$·H_2O versus EME·H_2O. The primary sources of these differences, according to the LED results, stem from the higher dispersion interaction with the introduced methyl group and from a large gain in the charge-transfer component. The present quantum chemical calculations correlate very well with the experimental observations for the out-of-plane libration bands of this series of water complexes, unlike in the comparison of the EME-PME pair. The calculated O-H stretching band origins show that the PME·H_2O complex has a larger red-shift relative to the EME·H_2O complex. This suggests that the out-of-plane librational band position is more sensitive to the electrostatics and the N/D components of the electronic correlation and therefore appears to provide a somewhat better probe of the localized intermolecular hydrogen bond itself, rather than the cumulative interaction energy, at least when fine differences in the structure and dispersion energy are present. This conclusion seems to be supported by the out-of-plane librational signatures for the TBME·H_2O and DIPE·H_2O complexes where the observed band origin for the latter system is significantly smaller despite the overall higher dissociation energy. On the contrary, the local energy decomposition approach shows that the TBME·H_2O interaction contains the larger non-dispersive energy contribution. For cases where the bonding is highly similar and the energy differences are high, e.g. in the series of symmetrical ethers, a high degree of linearity with respect to the theoretical D_0-values is observed. This is likely one of the sources of the remarkably linear relationship between observed out-of-plane HF librational band origins and the square root of the respective experimental binding energies ($D_0 \propto \nu^2_{oop}$) reported previously for a series of linear hydrogen-bonded HF complexes by Klemperer *et al.*[58]. The absolute band centers for the

TABLE II. The results of the computational analysis of the dissociation energies for the binary complexes of water with ethers, aliphatic alcohols and the water dimer, using the LED method at the DLPNO-CCSD(T)/AV5Z level (units of kJ·mol^{-1}). The table includes the geometric preparation energy ΔE_{geo}, the electronic preparation (EP), the HF electrostatic and exchange terms (el.st+XC), the sum of the HF interaction terms ($\mathrm{Int_{ref}}$), the CCSD strong and weak pairs ($\mathrm{SP_{res.}}$ and WP), the pure dispersive contribution (Disp.) and the triples term (T). The total dispersive ($\mathrm{Total_{Disp}}$) and the non-dispersive ($\mathrm{Total_{N/D}}$) terms are indicated in bold. The total change of zero-point energies ΔZPE upon complexation are calculated at the MP2/AVQZ level in the harmonic approximation.

System	ΔE_{geo}	EP	el.st+XC	$\mathrm{Int_{ref}}$	$\mathrm{SP_{res}}$	WP	**$\mathrm{Total_{N/D}}$**	Disp	(T)	**$\mathrm{Total_{Disp}}$**	D_{e}	ΔZPE	D_0
H_2O	0.2	96.3	-111.5	-15.2	0.3	-0.07	**-14.9**	-5.2	-0.9	**-6.1**	-20.8	8.7	-12.1
DME	0.7	130.8	-145.2	-14.4	-0.3	-0.08	**-14.7**	-8.9	-1.5	**-10.4**	-24.4	7.4	-17.0
EME	0.7	142.7	-156.5	-13.8	-0.7	-0.09	**-14.6**	-10.3	-1.8	**-12.1**	-25.9	7.7	-18.2
PME_{tg}	0.7	141.6	-155.7	-14.0	-0.8	-0.10	**-13.4**	-11.4	-1.8	**-13.1**	-25.8	7.4	-18.4
DEE	0.8	150.9	-164.6	-13.7	-0.3	-0.10	**-14.1**	-11.9	-2.0	**-13.9**	-27.2	7.9	-19.3
DIPE	0.8	162.5	-176.4	-13.9	-0.6	-0.14	**-14.6**	-13.4	-2.2	**-15.6**	-29.4	8.1	-21.3
TBME	0.9	162.5	-176.5	-14.0	-0.7	-0.12	**-14.9**	-12.5	-2.1	**-14.6**	-28.5	8.3	-20.3
TBEE	1.1	172.1	-184.3	-12.2	-1.1	-0.15	**-13.4**	-14.4	-2.5	**-16.9**	-29.3	8.6	-20.7
MeOH	0.5	116.5	-131.9	-15.4	0.7	-0.09	**-14.9**	-7.9	-1.3	**-9.2**	-23.6	7.7	-15.9
EtOH_{g+}	1.2	132.5	-147.8	-15.3	0.7	-0.08	**-14.8**	-10.5	-1.6	**-12.1**	-25.7	8.1	-17.6
EtOH_{t}	0.6	130.0	-144.9	-15.0	0.6	-0.10	**-14.4**	-9.7	-1.6	**-11.3**	-25.1	7.9	-17.2
i-POH	0.7	142.2	-156.9	-14.7	0.5	-0.11	**-14.3**	-11.5	-1.8	**-13.3**	-26.9	8.3	-18.7
t-BuOH	0.7	146.5	-161.6	-15.2	0.7	-0.13	**-14.6**	-12.0	-1.9	**-13.8**	-27.7	8.3	-19.4

out-of-plane HF librational transitions were shown to be more reliable measures of the intermolecular hydrogen bond energies D_0 than the traditional complexation redshifts of the intramolecular HF stretching bands relative to the free HF molecule.

V. CONCLUSIONS

The interplay of non-covalent intermolecular forces involved in the micro-solvation of seven different aliphatic ether molecules with systematically varied alkyl substituents has been explored by far-infrared neon matrix isolation spectroscopy in combination with explorative quantum chemical modeling. The primary focus experimentally has been to recover the very informative band origins for the highly anharmonic intermolecular out-of-plane librational transitions of this series of hydrogen-bonded ether-water complexes to complement previous far-infrared investigations of more simple alcohol-water complexes. The out-of-plane librational motion of the first solvating water molecule involves a significant change of the water dipole moment and gives rise to strong characteristic far-infrared bands in the range from 546 cm^{-1} to 574 cm^{-1}, which are correlated quantitatively with the intermolecular ether-water complexation energies with our currently best feasible theoretical estimates, excluding anharmonic corrections, ranging from 17.0 (DME·H_2O) to 21.3 kJ·mol^{-1} (DIPE·H_2O). For the energetically close complexes, a fine interplay between secondary dispersive interactions and the primary intermolecular hydrogen bonds has been revealed, which is poorly predicted by the commonly used scalable electronic structure methodologies. For the larger asymmetric systems, the directional intermolecular hydrogen bonds are in direct competition with non-directional dispersion forces comprising almost half of the total interaction energy D_{e}. The local energy decomposition of the interaction energies shows that the net non-dispersive component decreases with the size of the substituents caused by the increased electrostatic repulsion of the fragments. The present contribution suggests that the absolute out-of-plane librational band position is more closely linked to the electrostatics and the N/D components of the electronic correlation. This observable appears to provide a somewhat better probe of the localized and directional intermolecular hydrogen bonds rather than the less directional cumulative intermolecular binding motifs. The presented data set provides rigorous experimental benchmark points for further improvement of high-level *ab initio* electronic structure methods in the field of non-covalent interactions. The conventional RI-MP2 approach with the AVQZ basis set shows good consistency for predictions of the relative alkyl substituent effect when calibrated with experimental data for closely related systems, which allows to remove the uncertainty associated with anharmonicity. The present work has been limited to linear and branched alkyl substituents that are all resulting in an $+I$ inductive effect and thereby increased hydrogen bond acceptor capability of the O atoms compared to the smallest DME·H_2O system and the water dimer. The next step in further investigations of the aforementioned correlations would be to study analogous ether-water systems containing more complex substituents, e.g. alkenyl and aryl fragments, tuning the acceptor fragments and shifting the balance

of electrostatic and dispersive forces, as well as expanding the range of the set towards lower interaction energies.

VI. SUPPLEMENTARY MATERIAL

The supplementary material contains a description of the local energy decomposition (LED) procedure, the XYZ coordinates of the optimized structures, the graphic representations of the conformations of the DIPE and DEE complexes with water and the relevant ORCA output files containing the harmonic vibrational frequencies.

VII. ACKNOWLEDGEMENTS

The authors acknowledge financial support provided by the Danish Hydrocarbon Research & Technology Centre (DHRTC) at DTU as part of the "AWF.1 Reservoir Fluids Characterization" work package. The authors are grateful to the DTU Computing Center for access to the high-performance computing (HPC) services and the technical support provided. Finally, the mechanical workshop at DTU Chemistry is acknowledged for help and advice in the designs of the experimental setups.

VIII. CONFLICTS OF INTEREST

There are no conflicts to declare.

[1] A. Luzar and D. Chandler, "Hydrogen-bond kinetics in liquid water," *Nature*, vol. 379, pp. 55–57, Jan. 1996.
[2] K. Fumino, A. Wulf, and R. Ludwig, "Strong, localized, and directional hydrogen bonds fluidize ionic liquids," *Angewandte Chemie*, vol. 47, pp. 8731–8734, Oct. 2008.
[3] W. T. S. Cole, R. S. Fellers, M. R. Viant, C. Leforestier, and R. J. Saykally, "Far-infrared VRT spectroscopy of the water dimer: Characterization of the 20 μm out-of-plane librational vibration," *The Journal of Chemical Physics*, vol. 143, p. 154306, Oct. 2015.
[4] W. T. S. Cole, R. S. Fellers, M. R. Viant, and R. J. Saykally, "Hydrogen bond breaking dynamics in the water pentamer: Terahertz VRT spectroscopy of a 20 μm libration," *The Journal of Chemical Physics*, vol. 146, p. 014306, Jan. 2017.
[5] W. T. S. Cole, J. D. Farrell, A. A. Sheikh, Öezlem Yönder, R. S. Fellers, M. R. Viant, D. J. Wales, and R. J. Saykally, "Terahertz VRT spectroscopy of the water hexamer-d12 prism: Dramatic enhancement of bifurcation tunneling upon librational excitation," *The Journal of Chemical Physics*, vol. 148, p. 094301, Mar. 2018.
[6] F. N. Keutsch, R. S. Fellers, M. G. Brown, M. R. Viant, P. B. Petersen, and R. J. Saykally, "Hydrogen bond breaking dynamics of the water trimer in the translational and librational band region of liquid water," *Journal of the American Chemical Society*, vol. 123, pp. 5938–5941, June 2001.
[7] F. N. Keutsch, R. S. Fellers, M. R. Viant, and R. J. Saykally, "Far-infrared laser vibration–rotation–tunneling spectroscopy of water clusters in the librational band region of liquid water," *The Journal of Chemical Physics*, vol. 114, pp. 4005–4015, Mar. 2001.
[8] D. Mihrin, J. Andersen, P. W. Jakobsen, and R. W. Larsen, "Highly localized H_2O librational motion as a far-infrared spectroscopic probe for microsolvation of organic molecules," *Physical Chemistry Chemical Physics*, vol. 21, no. 4, pp. 1717–1723, 2019.
[9] J. Andersen, J. Heimdal, and R. W. Larsen, "Spectroscopic identification of ethanol-water conformers by large-amplitude hydrogen bond librational modes," *The Journal of Chemical Physics*, vol. 143, p. 224315, Dec. 2015.
[10] S. Marriott and R. D. Topsom, "Theoretical studies of the inductive effect. IV. A theoretical scale of substituent field parameters," *Journal of the American Chemical Society*, vol. 106, pp. 7–10, Jan. 1984.
[11] K. Fumino, V. Fossog, P. Stange, D. Paschek, R. Hempelmann, and R. Ludwig, "Controlling the subtle energy balance in protic ionic liquids: Dispersion forces compete with hydrogen bonds," *Angewandte Chemie International Edition*, vol. 54, pp. 2792–2795, Jan. 2015.
[12] A. G. P. Maloney, P. A. Wood, and S. Parsons, "Competition between hydrogen bonding and dispersion interactions in the crystal structures of the primary amines," *CrystEngComm*, vol. 16, no. 19, pp. 3867–3882, 2014.
[13] T. J. Wallington, P. Dagaut, R. Liu, and M. J. Kurylo, "Gas-phase reactions of hydroxyl radicals with the fuel additives methyl *tert*-butyl ether and *tert*-butyl alcohol over the temperature range 240-440 K," *Environmental Science & Technology*, vol. 22, pp. 842–844, July 1988.
[14] K. Watanabe, "The toxicological assessment of cyclopentyl methyl ether (CPME) as a green solvent," *Molecules*, vol. 18, pp. 3183–3194, Mar. 2013.
[15] R. R. Ratnakar, B. Dindoruk, and L. Wilson, "Experimental investigation of DME–water–crude oil phase behavior and PVT modeling for the application of DME-enhanced waterflooding," *Fuel*, vol. 182, pp. 188–197, Oct. 2016.
[16] A. Williamson, "XLV. Theory of ætherification," *The London, Edinburgh, and Dublin Philosophical Magazine and Journal of Science*, vol. 37, pp. 350–356, Nov. 1850.
[17] J. Casanova, "Student preparation and manipulation of a gas — methyl ethyl ether," *Journal of Chemical Education*, vol. 40, p. 41, Jan. 1963.
[18] J. Andersen, J. Heimdal, B. Nelander, and R. W. Larsen, "Competition between weak OHÂ·Â·Â·π and CHÂ·Â·Â·O hydrogen bonds: THz spectroscopy of the C_2H_2â"H_2O and C_2H_4â"H_2O complexes," *The Journal of Chemical Physics*, vol. 146, p. 194302, May 2017.
[19] J. Andersen, J. Heimdal, D. W. Mahler, B. Nelander, and R. W. Larsen, "Communication: THz absorption spectrum of the CO_2–H_2O complex: Observation and assignment of intermolecular van der Waals vibrations," *The Journal of Chemical Physics*, vol. 140, p. 091103, Mar. 2014.
[20] J. Andersen, A. Voute, D. Mihrin, J. Heimdal, R. W. Berg, M. Torsson, and R. W. Larsen, "Probing the global potential energy minimum of $(CH_2O)_2$: THz absorption spectrum of $(CH_2O)_2$ in solid neon and *para*-hydrogen," *The Journal of Chemical Physics*, vol. 146, p. 244311, June 2017.
[21] F. Neese, "Software update: the ORCA program system, version 4.0," *WIREs Computational Molecular Science*, vol. 8, p. e1327, July 2017.
[22] D. E. Bernholdt and R. J. Harrison, "Large-scale correlated electronic structure calculations: the RI-MP2 method on parallel computers," *Chemical Physics Letters*, vol. 250, pp. 477–484, Mar. 1996.
[23] R. A. Kendall, T. H. Dunning, and R. J. Harrison, "Electron affinities of the first-row atoms revisited. systematic basis sets and wave functions," *The Journal of Chemical Physics*, vol. 96, pp. 6796–6806, May 1992.
[24] F. Neese, F. Wennmohs, A. Hansen, and U. Becker, "Efficient, approximate and parallel Hartree–Fock and hybrid DFT calculations. A 'chain-of-spheres' algorithm for the Hartree–Fock exchange," *Chemical Physics*, vol. 356, pp. 98–109, Feb. 2009.
[25] S. Kossmann and F. Neese, "Efficient structure optimization with second-order many-body perturbation theory: The RIJCOSX-MP2 method," *Journal of Chemical Theory and Computation*, vol. 6, pp. 2325–2338, July 2010.

[26]F. Weigend, "A fully direct RI-HF algorithm: Implementation, optimised auxiliary basis sets, demonstration of accuracy and efficiency," *Physical Chemistry Chemical Physics*, vol. 4, pp. 4285–4291, sep 2002.

[27]F. Weigend, "Accurate coulomb-fitting basis sets for H to Rn," *Physical Chemistry Chemical Physics*, vol. 8, no. 9, p. 1057, 2006.

[28]F. Weigend, "Hartree–fock exchange fitting basis sets for H to Rn," *Journal of Computational Chemistry*, vol. 29, no. 2, pp. 167–175, 2007.

[29]F. Weigend, A. Köhn, and C. Hättig, "Efficient use of the correlation consistent basis sets in resolution of the identity MP2 calculations," *The Journal of Chemical Physics*, vol. 116, pp. 3175–3183, Feb. 2002.

[30]C. M. Breneman and K. B. Wiberg, "Determining atom-centered monopoles from molecular electrostatic potentials. the need for high sampling density in formamide conformational analysis," *Journal of Computational Chemistry*, vol. 11, pp. 361–373, Apr. 1990.

[31]A. Schäfer, A. Klamt, D. Sattel, J. C. W. Lohrenz, and F. Eckert, "COSMO implementation in TURBOMOLE: Extension of an efficient quantum chemical code towards liquid systems," *Physical Chemistry Chemical Physics*, vol. 2, no. 10, pp. 2187–2193, 2000.

[32]C. Riplinger, P. Pinski, U. Becker, E. F. Valeev, and F. Neese, "Sparse maps—a systematic infrastructure for reduced-scaling electronic structure methods. II. linear scaling domain based pair natural orbital coupled cluster theory," *The Journal of Chemical Physics*, vol. 144, p. 024109, Jan. 2016.

[33]C. Riplinger, B. Sandhoefer, A. Hansen, and F. Neese, "Natural triple excitations in local coupled cluster calculations with pair natural orbitals," *The Journal of Chemical Physics*, vol. 139, p. 134101, Oct. 2013.

[34]D. G. Liakos, M. Sparta, M. K. Kesharwani, J. M. L. Martin, and F. Neese, "Exploring the accuracy limits of local pair natural orbital coupled-cluster theory," *Journal of Chemical Theory and Computation*, vol. 11, pp. 1525–1539, Mar. 2015.

[35]W. B. Schneider, G. Bistoni, M. Sparta, M. Saitow, C. Riplinger, A. A. Auer, and F. Neese, "Decomposition of intermolecular interaction energies within the local pair natural orbital coupled cluster framework," *Journal of Chemical Theory and Computation*, vol. 12, pp. 4778–4792, Sept. 2016.

[36]A. Altun, F. Neese, and G. Bistoni, "Effect of electron correlation on intermolecular interactions: A pair natural orbitals coupled cluster based local energy decomposition study," *Journal of Chemical Theory and Computation*, vol. 15, pp. 215–228, Nov. 2018.

[37]J. R. Durig and J. S. Church, "Low frequency vibrational spectra, barriers to methyl rotations and lattice modes of diethylether," *Molecular Crystals and Liquid Crystals*, vol. 69, pp. 217–240, July 1981.

[38]N. Kuze, N. Kuroki, H. Takeuchi, T. Egawa, and S. Konaka, "Structural and conformational analysis of diethyl ether by molecular orbital constrained electron diffraction combined with microwave spectroscopic data," *Journal of Molecular Structure*, vol. 301, pp. 81–94, Dec. 1993.

[39]J. Ceponkus and B. Nelander, "Water dimer in solid neon. Far-infrared spectrum," *The Journal of Physical Chemistry A*, vol. 108, pp. 6499–6502, Aug. 2004.

[40]J. Ceponkus, G. Karlström, and B. Nelander, "Intermolecular vibrations of the water trimer, a matrix isolation study," *The Journal of Physical Chemistry A*, vol. 109, pp. 7859–7864, Aug. 2005.

[41]J. Ceponkus, P. Uvdal, and B. Nelander, "On the structure of the matrix isolated water trimer," *The Journal of Chemical Physics*, vol. 134, p. 064309, Feb. 2011.

[42]K. Taga, K. Kawasaki, Y. Yamamoto, T. Yoshida, K. Ohno, and H. Matsuura, "Raman spectra and conformational analyses for a series of diethyl ether and its organosilicon derivatives, $CH_3MH_2OM'h_2CH_3$ (M, M'=C and Si), by density functional theory," *Journal of Molecular Structure*, vol. 788, pp. 159–175, May 2006.

[43]R. Snyder and G. Zerbi, "Vibrational analysis of ten simple aliphatic ethers: Spectra, assignments, valence force field and molecular conformations," *Spectrochimica Acta Part A: Molecular Spectroscopy*, vol. 23, pp. 391–437, Feb. 1967.

[44]K. Beć, A. Muszyński, N. Michniewicz, W. Wrzeszcz, A. Kotynia, and J. Hawranek, "Vibrational spectra of liquid di-isopropylether," *Vibrational Spectroscopy*, vol. 55, pp. 44–48, Jan. 2011.

[45]A. Clague and A. Danti, "Low frequency infrared and raman spectra of certain aliphatic ethers," *Spectrochimica Acta Part A: Molecular Spectroscopy*, vol. 24, pp. 439–442, Apr. 1968.

[46]T. Kitagawa, K. Ohno, H. Sugeta, and T. Miyazawa, "Far infrared spectra and internal-rotation potential of ethyl methyl ether," *Bulletin of the Chemical Society of Japan*, vol. 45, pp. 969–975, Apr. 1972.

[47]J. R. Durig, Y. Jin, H. V. Phan, J. Liu, and D. T. Durig, "Far-infrared spectra, conformational stability, barriers to internal rotation, *ab anitio* calculations, r_0 structural parameters, and vibrational assignment of ethyl methyl ether," *Structural Chemistry*, vol. 13, no. 1, pp. 1–26, 2002.

[48]T. Shimanouchi, Y. Ogawa, M. Ohta, H. Matsuura, and I. Harada, "Vibration spectra and rotational isomerism of chain molecules. I. Methyl propyl ether, ethyl propyl ether, and butyl methyl ether," *Bulletin of the Chemical Society of Japan*, vol. 49, pp. 2999–3008, Nov. 1976.

[49]K. Beć, A. Kwiatek, and J. Hawranek, "Vibrational analysis of neat liquid tert-butylmethylether," *Journal of Molecular Liquids*, vol. 196, pp. 26–31, Aug. 2014.

[50]T. Egawa, H. Moriyama, H. Takeuchi, S. Konaka, K. Siam, and L. Schäfer, "Structural study and conformational analysis of *t*-butyl ethyl ether by gas electron diffraction, *ab initio* calculations and vibrational spectroscopy," *Journal of Molecular Structure*, vol. 298, pp. 37–45, Oct. 1993.

[51]A. Engdahl and B. Nelander, "Intermolecular vibrations of the dimethyl ether–water complex. A matrix isolation study," *J. Chem. Soc., Faraday Trans.*, vol. 88, no. 2, pp. 177–182, 1992.

[52]S. W. Han and K. Kim, "Infrared matrix isolation and ab initio quantum mechanical study of dimethyl ether–methanol complex," *Journal of Molecular Structure*, vol. 475, pp. 43–53, Jan. 1999.

[53]M. Heger, J. Andersen, M. A. Suhm, and R. W. Larsen, "The donor OH stretching–libration dynamics of hydrogen-bonded methanol dimers in cryogenic matrices," *Physical Chemistry Chemical Physics*, vol. 18, no. 5, pp. 3739–3745, 2016.

[54]J. Andersen, J. Heimdal, and R. W. Larsen, "The influence of large-amplitude librational motion on the hydrogen bond energy for alcohol–water complexes," *Physical Chemistry Chemical Physics*, vol. 17, no. 37, pp. 23761–23769, 2015.

[55]A. Altun, F. Neese, and G. Bistoni, "Local energy decomposition analysis of hydrogen-bonded dimers within a domain-based pair natural orbital coupled cluster study," *Beilstein Journal of Organic Chemistry*, vol. 14, pp. 919–929, Apr. 2018.

[56]H. I. Rivera-Arrieta, J. M. Turney, and H. F. Schaefer, "Structural distortions accompanying noncovalent interactions: Methane–water, the simplest C–H hydrogen bond," *Journal of Chemical Theory and Computation*, vol. 13, pp. 1478–1485, Feb. 2017.

[57]G. Bistoni, A. A. Auer, and F. Neese, "Understanding the role of dispersion in frustrated Lewis pairs and classical Lewis adducts: A domain-based local pair natural orbital coupled cluster study," *Chemistry - A European Journal*, vol. 23, pp. 865–873, Dec. 2016.

[58]Z. Yu and W. Klemperer, "Asymmetry in angular rigidity of hydrogen-bonded complexes," *Proceedings of the National Academy of Sciences*, vol. 102, pp. 12667–12669, Aug. 2005.

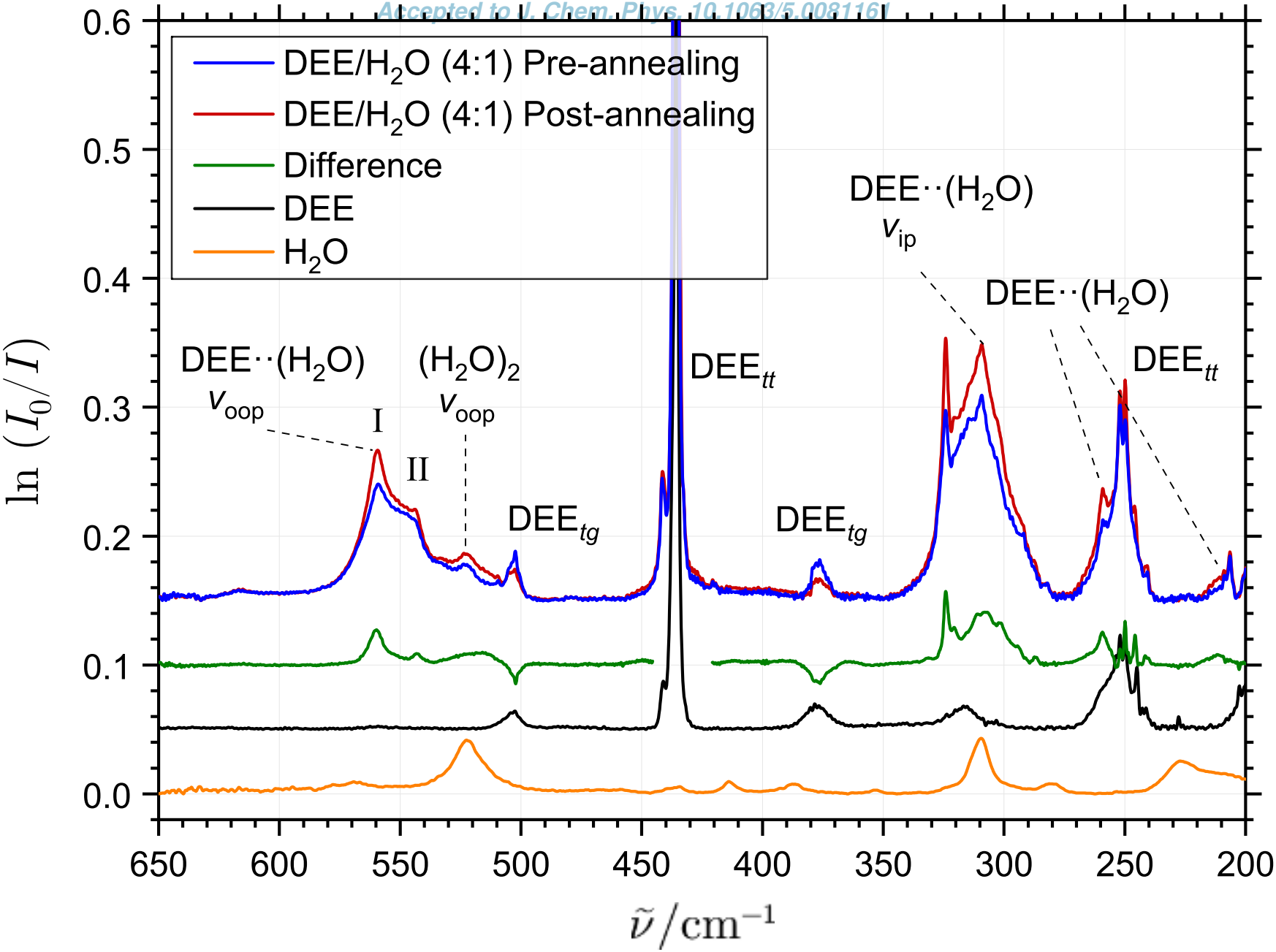

Accepted to J. Chem. Phys. 10.1063/5.0081161